INTERNATIONAL SOCIETY FOR SOIL MECHANICS AND GEOTECHNICAL ENGINEERING

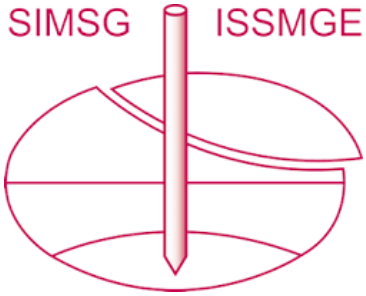

This paper was downloaded from the Online Library of the International Society for Soil Mechanics and Geotechnical Engineering (ISSMGE). The library is available here:

https://www.issmge.org/publications/online-library

This is an open-access database that archives thousands of papers published under the Auspices of the ISSMGE and maintained by the Innovation and Development Committee of ISSMGE.

The paper was published in the proceedings of the 13th International Symposium on Landslides and was edited by Miguel Angel Cabrera, Luis Felipe Prada-Sarmiento and Juan Montero. The conference was originally scheduled to be held in Cartagena, Colombia in June 2020, but due to the SARS-CoV-2 pandemic, it was held online from February 22nd to February 26th 2021.

Experimental study on failure of unsaturated homogeneous earthen slope under Even and Uneven rainfall patterns

Xianghua Song[1], Yong Tan[2], Weizhen Jiang[3]

[1] Ph.D. Candidate, Department of Geotechnical Engineering, College of Civil Engineering, Tongji University, 1239 Si-ping Road, Shanghai 200092, China. Email: 1710188@tongji.edu.cn

[2] Professor, Department of Geotechnical Engineering, College of Civil Engineering, Tongji University, 1239 Si-ping Road, Shanghai 200092, China. Email: tanyong21th@tongji.edu.cn

[3]Ph.D. Candidate, Department of Geotechnical Engineering, College of Civil Engineering, Tongji University, 1239 Si-ping Road, Shanghai 200092, China. Email: jiangweizhen@tongji.edu.cn

Abstract

Slope failures triggered by heavy rainfall are becoming a more pressing concern around the world. In previous studies, most researches on rainfall-induced slope failure focused on the constant rainfall pattern. However, in most natural rainstorm events, rainfall intensity is variable throughout the duration. To properly investigate rainfall-induced slope failure, more realistic uneven rainfall patterns are necessary. Therefore, a series of comparative experimental studies were conducted to investigate the distinctive effects of different rainfall patterns (constant rainfall pattern and unimodal rainfall pattern) on a homogenous earthen slope. The results of model tests show that the failure evolution models were affected significantly by the rainfall patterns and two types of failures were observed. By comparing the different slope failure process, retrogressive failure was observed under the constant rainfall pattern. While, in case of unimodal rainfall pattern, translational failure occurred suddenly without any local failure in advance. Under the same cumulative rainfall, the unimodal rainfall pattern produced more harmful influence on the earthen slope than the constant rainfall pattern, in terms of the erosion region of slope. In view of the change of pore water pressure with a characteristic of suddenness for a slope under the unimodal rainfall pattern, it was not recommended to take the traditional method of monitoring pore water pressure to predict slope failure. The findings and results yielded from experimental studies can help researchers and practitioners further understand the effect of rainfall patterns on rainfall-induced slope failures.

1 INTRODUCTION

According to the survey results, the economic losses by geological disasters exceeded 20 billion yuan every year in China, in which rainfall-induced slope failures accounted for 51% (Li et al. 2004). Rainfall reduces slope stability and threatens people's life and property. In recent years, many scholars have tried to find reasonable methods for predicting and take effective measures to prevent the occurrence of rainfall-induced slope failures (Caine 1980; Keefer et al. 1987; Iverson 2000; Stark et al. 2017; Tan et al. 2018). The mechanism of rainfall-induced slope failure caused by the mutual mechanical effect of soil and water has been explored. It has been generally recognized that the rapid rise of pore water pressure, seepage force, decreased matric suction, and consequently the reduced shear strength of soil, are critical to the initiation of the slope failures (Ochiai et al. 2004; Casiniet al.2010; Askrinejad et al. 2012; Stark & Hussain, 2013). Moreover, the warning threshold of cumulative rainfall or rainfall intensity has been established through statistical analysis of meteorological data and corresponding monitoring data of slope displacement, based on the principle of statistics (Casadei et al. 2003; Guzzetti et al. 2007). To date, many countries have proposed their own rainfall thresholds for landslides, e.g., 180 mm, 150 mm, 350 mm in American, Japan, Hong Kong, respectively (Chen et al. 2012). It has been widely recognized that short-term rainstorm and continuous long-duration rainfall are more serious to induce slope failure (Brunetti et al. 2010).

Till now, the influence of different rainfall patterns (i.e., rainfall intensity varies during a particular period) on slope failures has not received adequate attention in the above studies. On June 30, 1991, monitoring stations of Huang-la-shi slope in the Reservoir Region of the Yangtze Gorge had reported daily rainfall of up to 156 mm, and there was no landslide. Whereas, when the daily cumulative precipitation reached 133.6 mm on August 6, 1991, more than 20 collapses, landslides and debris flows happened near the area (Zhong 1998). Although the cumulative rainfall of the former was greater than that of the latter, the rainfall intensity of the latter was much more uneven, in which the heaviest rainfall was up to 75 mm in 1 hour. Apparently, in addition to cumulative precipitation, slope stability also depended greatly on the rainfall patterns. In light of this, this study carried out a series of experiments to investigate the effect of rainfall patterns on slope stability. Not only the detailed observations of failure process, failure evolution modes, and settlement of slope crest, but also with the particular emphasis on the change in pore water pressure and infiltration rate, were measured in the experiment. The findings and results yielded from the experiment can help researchers and practitioners further understand the effect of rainfall patterns on rainfall-induced slope failures.

2 EXPERIMENTAL APPARATUS

The rainfall experimental model consisted of an experiment tank, a rainfall control system, camera equipment, and a drain system. The whole experiment tank was 1.6 m long, 0.6 m wide, and 1.0 m high, in which there were two water chambers 0.2 m wide on both sides for facilitating observation of water level. Holes were reserved on the middle dummy plates in advance and a layer of thin gauze was glued on the inner side to prevent sand from flowing away through the holes. The rainfall simulator was set up 0.6 m above the model slope and rainwater was atomized through the nozzles to simulate rainstorm. The amount of water flowing through the simulator was controlled through a regulator. Additionally, the accumulated rainwater can be drained freely through the drainage pipe at the bottom of experiment tank.

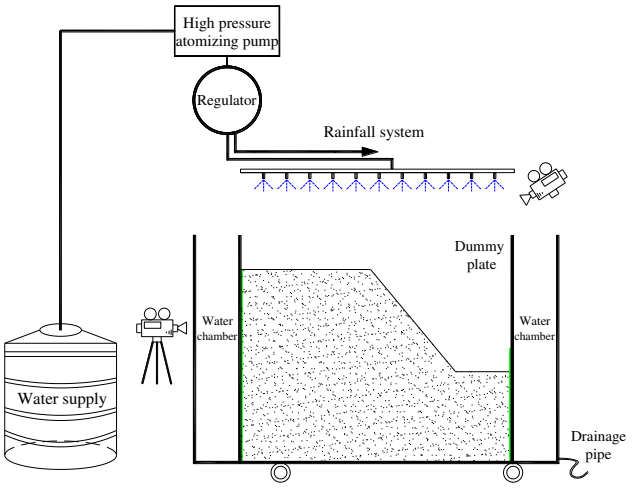

Figure 1. Configuration of the indoor rainfall model experiment.

3 PROPERTIES OF EXPERIMENT SOIL

In the experiment, Fujian standard sand was used to construct the slope models since it was convenient to prepare the model slopes with the relatively uniform property. After a series of

measurement tests, the parameters of the soil were summarized in Table 1.

Table 1. Properties of soil samples.

	$\rho_{d,max}$	w(%)	d (mm)	C_u	C_c	k_s(cm/s)	ϕ'(°)
Sand	1.70	17.2	0.08~2.0	4.72	0.38	7.66×10^{-3}	40.7

4 EXPERIMENTAL PROGRAM

After considering the connection between the size of real soil slope and model slope in the laboratory, a similarity ratio of 1:10 was determined for the slope model and the soil slope of 0.8 m high was constructed by placing the soil with medium compaction to maintain uniform soil characteristics. Before the experiment, a pilot rainfall process was carried out first to simulate the water distribution of the soil layer in its natural state. The angle of experimental slope (50°) with a safety factor of 1.2 was calculated by the SLOPE/W software (SLOPE/W 2012), in which the suction of natural unsaturated sand was considered in analysis. Additionally, four thin layers of red-sands were added to show the displacement of the slope soils. Some colored solid dyes without any effect on slope soil were pre-buried in the slope crest to track the seepage line of rainwater infiltration.

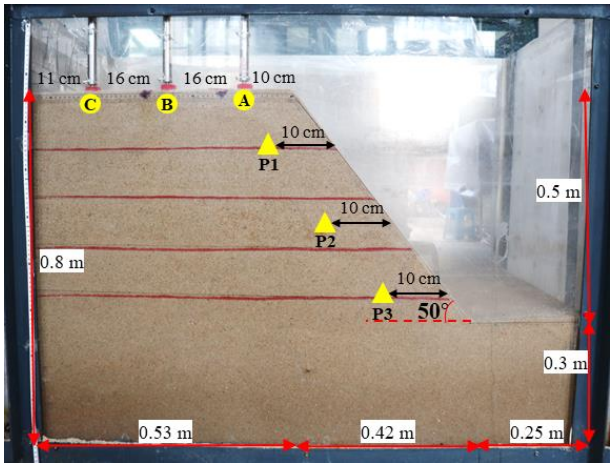

Figure 2. Dimensions and monitoring points for the earthen slope model under rainfall.

Three displacement sensors measuring the settlement displacement were placed on the slope crest, marked as **A~C** in Fig.2. Three pore water pressure sensors named **P1~P3** were buried in advance to measure the change in pore water pressure.

By analyses of rainfall data available from Chinese southeast coastal regions, two typical rainfall patterns (constant and unimodal) were selected for experimental testing. During the rainy season, rainstorm was very common and average daily precipitation in such rain days was usually more than 150 mm or even 200 mm. Considering that a long duration interval would result in few time intervals with very low rainfall intensities, which caused difficulties in distinguishing different rainfall patterns. Thereby, in order to highlight the effects of different rainfall patterns on the slope, 200 mm was determined to represent the cumulative precipitation. Meanwhile, the duration of the rainfall was selected to be 60 minutes and was divided into six-time spans in this study, as shown in Fig.3.

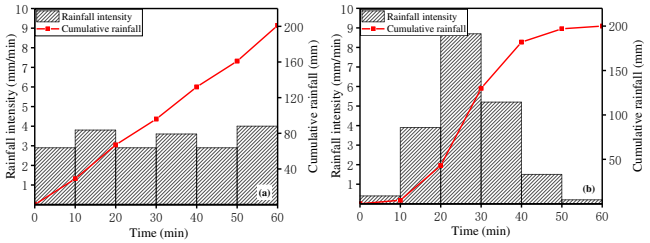

Figure 3. Designed rainfall patterns: (a) constant rainfall; (b) unimodal rainfall.

The parameters of each experiment were shown in Table 2.

Table 2. The initial properties of experimental slopes.

	Sand density (g/cm^3)	Total rainfall (mm)	Slope angle (°)	W(%)	Rainfall pattern
Slope A	1.729	200	50	4.4	Constant
Slope B	1.702	200	50	4.3	Unimodal

5 EXPERIMENT RESULTS AND DISCUSSION

In this study, the failure process, failure evolution modes, settlement of slope crest, pore water pressure, and seepage velocity subjected to different rainfall patterns (constant rainfall and unimodal rainfall) were recorded for analysis.

5.1 Failure process

Fig.4 shows the failure process of the slope model under constant rainfall, in which its cumulative rainfall was 200 mm and rainfall intensity was shown in Fig.3 (a).

As the experiment began, the rainwater infiltrated into the slope instantly and flowed toward its base gradually, the orientation of wetting front turned parallel to the horizontal base, shown by the liquefied red dyes. During the period, there was no runoff observed on the slope surface, because the infiltration capacity of the sand layer was higher than the rainfall intensities used in this study.

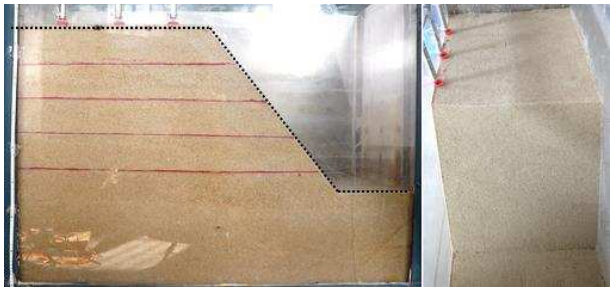

(a) t=0s

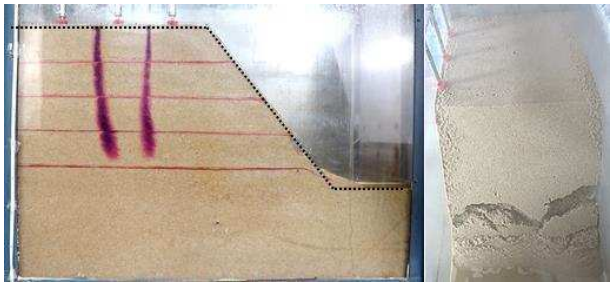

(b) t=25 min

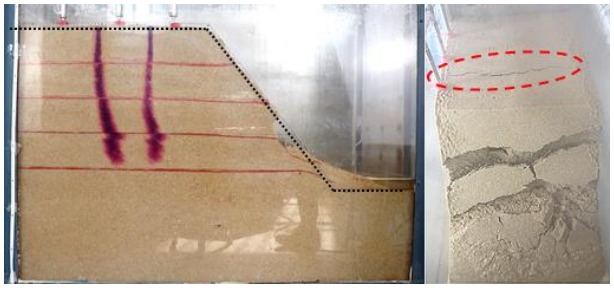

(c) t=29 min 13 s

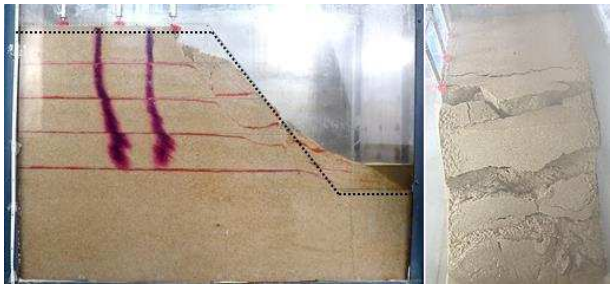

(d) t=31 min

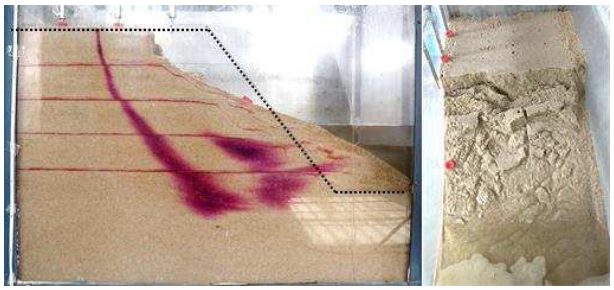

(e) t=60 min

Figure 4. Failures of slope model under the constant rainfall.

After the wetting front reached the base, with the rising of saturation degree, flow slide failure appeared near the slope toe, indicating the initiation of slope failure, see Fig.4 (b). With continuing of rainfall, the soil of slope surface gradually fell off in blocks, the area of displacement influence expanded from the slope toe to the top, until a tension crack occurred at the slope crest, as shown in Fig.4 (c). Finally, at 29 min 13 s, the soil shear strength along the sliding surface was insufficient to retain the upper slope and a global failure with a straight sliding surface happened suddenly, as shown from the displacement of red sand on the side in Fig.4 (d). At last, the final shape of the slope model under the constant rainfall pattern was shown in Fig.4 (e).

Fig.5 shows the failure process of slope model under unimodal rainfall, in which its cumulative rainfall was 200 mm and rainfall intensity was shown in Fig.3 (b).

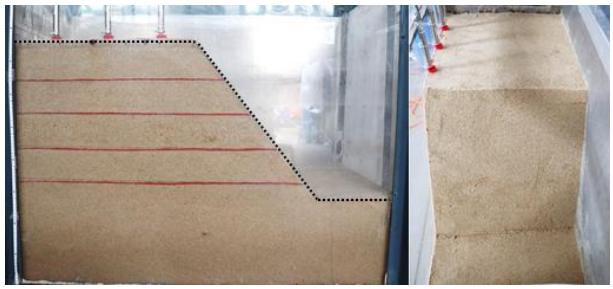

(a) t=0 s

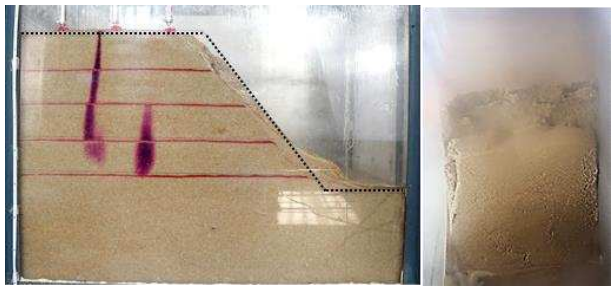

(b) t=24 min

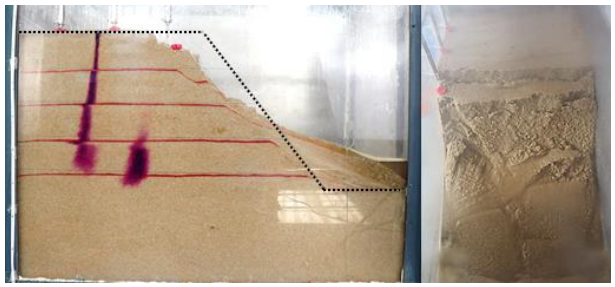

(c) t=26 min

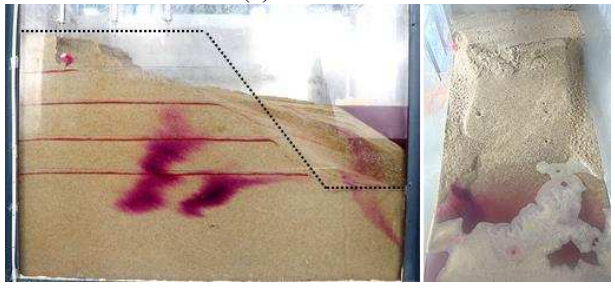

(d) t=60 min

Figure 5. Failures of slope model under unimodal rainfall

As rainfall lasted for 24 minutes, the slope suddenly underwent a translational failure featuring a linear sliding surface without any local failures in advance, see Fig.5 (b). Note that the global failure occurred when the rainfall intensity reached the peak value during the unimodal rainfall. With continuing of rainfall, a second global slide failure occurred 2 minutes later. Meanwhile, the phenomenon of runoff can be seen above the slope surface, because the rainfall intensity was higher than the infiltration capacity of the sand layer (7.66×10^{-3} cm/s) during the period of maximum rainfall intensity (8.7 mm/min = 14.5×10^{-3} cm/s). The area of slope failure expanded with continuing of rainfall, and the final obvious eroded area of slope failure was shown in Fig.5 (d).

In the experiment, two types of failures could be observed under the two different rainfall patterns. In the case of the constant rainfall pattern, with an initial slope failure occurring firstly near the slope toe, the downslope soil gradually slid under the effect of both gravity and rainwater seepage force. And then, the upper slope soil lost its vertical support and fell off in a short time, with a characteristic of sequential retrogressive failure, resulting in an occurrence of global failure suddenly in the end. While in the experiment with a unimodal rainfall pattern, the maximum rainfall intensity during the heaviest rainfall intensity played an important role in the process of slope failure. With continuing of rainfall, the shear strength of slope soil gradually reduced by the loss of capillarity cohesion due to the saturation. Under the joint effect of seepage force and gravity, the reduced shear strength was insufficient to maintain the stability of the entire slope until a translational failure happened suddenly. Therefore, it can be seen that the failure evolution mode of slope was greatly affected by different rainfall patterns. Retrogressive slope failure occurred under the constant rainfall pattern, while translational failure occurred under the unimodal rainfall pattern.

5.2 Slope erosion profiles

Fig.6 shows the development of slope erosion profiles over time under different rainfall patterns.

As shown in the slope erosion lines, local failures occurred firstly near the slope toe under the constant rainfall pattern. With continuing of rainfall, the range of failure area gradually expanded to the slope crest until the occurrence of global failure. The maximum distance between the sliding surface and initial slope surface was up to $0.22\,H_e$ (H_e - slope height). At the end of the experiment, the maximum erosion distance of slope crest was $0.3H_e$.

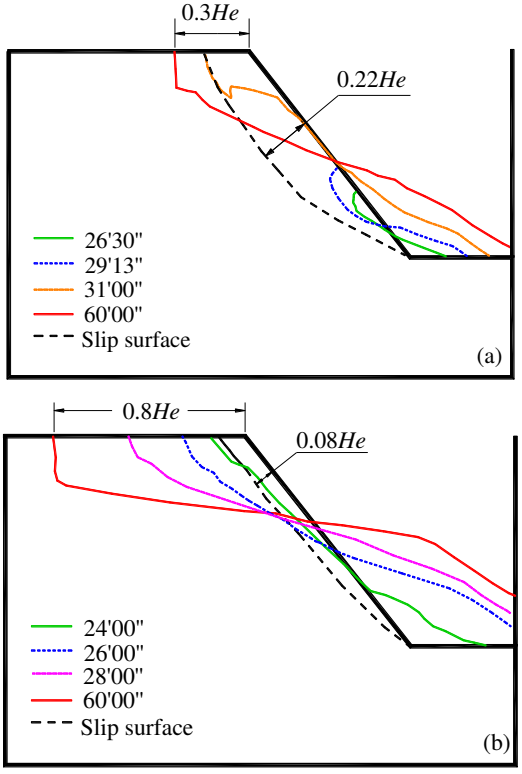

Figure 6. Slope erosion lines development over time under different rainfall patterns: (a) constant rainfall; (b) unimodal rainfall.

In the case of the unimodal rainfall pattern, translational failure featuring a straight sliding surface happened firstly with thickness of only $0.08H_e$ wide, which was much thinner than that of global slope failure in the constant rainfall. As rainfall went on, more and more eroded upper slope soils flowed from the slope crest to the slope toe, especially during the heaviest rainfall intensity. At last, the maximum failure distance of slope crest was up to $0.8\,H_e$, which was much larger than that in the constant rainfall pattern.

The above analyses show that the unimodal rainfall pattern was more harmful to earthen slope than the constant rainfall pattern.

5.3 Settlement displacement of slope crest

Fig.7 shows the settlement displacement of monitoring points at the slope crest under different rainfall patterns. Three displacement sensors with a maximum measuring range of 20 mm were installed at the top of the experiment tank, as shown in Fig.2.

When the slope model under the constant rainfall pattern, the initial slope failure near the slope toe occurred at 25 minutes and global slide

failure happened suddenly 6 minutes later. With the occurrence of initial failure, the settlements of 3.3 mm at point A, 2.5 mm at point B, and 1.9 mm at point C were measured. Throughout the entire rainfall experiment, point A was collapsed with the global slope failure at the 31 minutes, the settlements were 6.2 mm at point B and 4.4 mm at point C. Note that the settlement curves of point B and point C showed a characteristic of nonlinearity during the experiment of the constant rainfall pattern.

For slope under the unimodal rainfall pattern, translational failure occurred suddenly at 24 minutes with the collapse of point A, followed by point B and point C. As shown in Fig.7 (b), the time of global failure occurring correlated well with the heaviest rainfall intensity under the unimodal rainfall pattern.

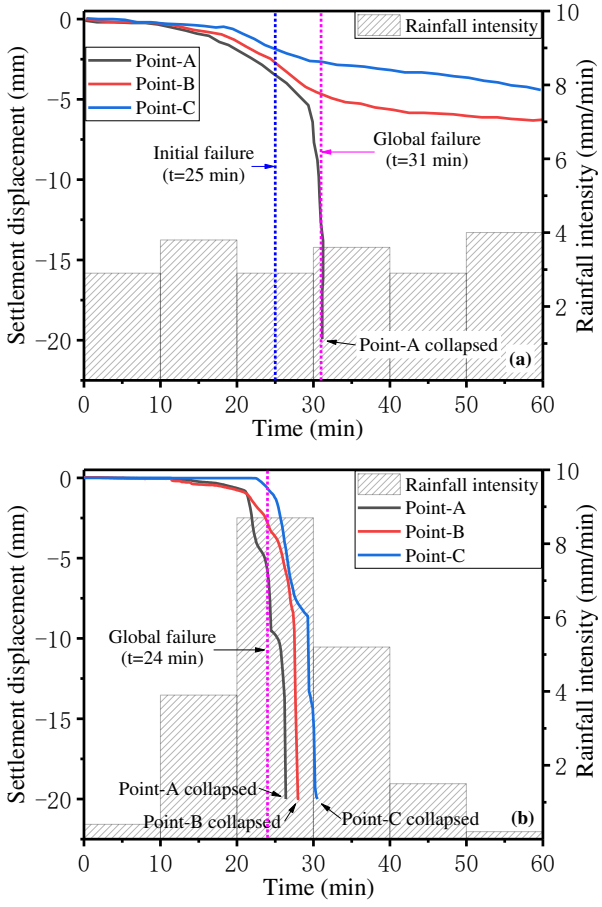

Figure 7. Settlement displacement of monitoring points on the slope top under different rainfall patterns: (a) constant rainfall; (b) unimodal rainfall.

The analyses above indicated that it was available to predict the slope failure by monitoring the settlement of slope crest in case of constant rainfall pattern. However, it was not suitable for a slope under unimodal rainfall because the sliding failure was abrupt and unexpected.

5.4 Pore-water pressure

Fig. 8 shows the increment of pore water pressure (PWP) measured at P1, P2, and P3 under the different rainfall patterns. Three pore pressure sensors were pre-buried close to the slope surface, as shown in Fig.2.

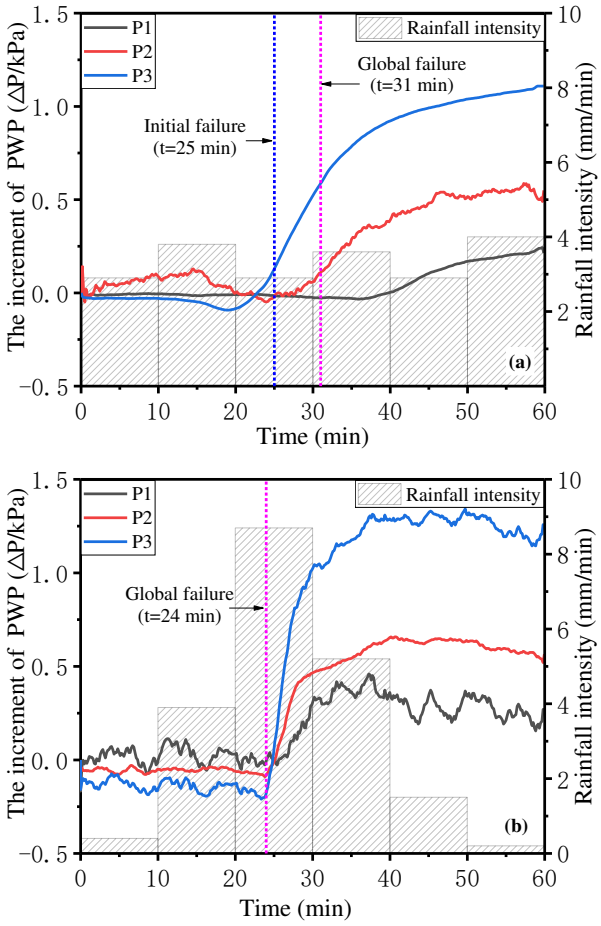

Figure 8. The increment of pore water pressure under different rainfall patterns: (a) constant rainfall; (b) unimodal rainfall.

For the slope under the constant rainfall pattern, the increment of PWP at P1, P2, and P3 stayed constant in the early period. Before the occurrence of initial failure, the pore pressure at point P3 had a slight rise due to the generation of excess pore pressure near the slope toe. Because of different locations, the change value of PWP at P3 close to the slope toe increased firstly and rose to 1.1 kPa in the end, followed by the point P2 with an increment of 0.55 kPa near the middle slope and point P1 close to the slope crest increased by 0.2 kPa. It's worthwhile to note that when the pore water pressure of P3 started to increase, the time was earlier than that of the occurrence of initial failure under the constant rainfall pattern. Based on this point, it was suggested that monitoring of the fluctuation of pore water pressure in a real

slope may give an indication of its inherent stability.

When the slope model was under the unimodal rainfall pattern, the development trends of pore water pressure were almost similar. In Fig.8 (b), the PWP value of P1, P2, and P3 stayed constant in the early stage but then increased suddenly with the occurrence of global slide failure at 24 minutes. The maximum increase in pore water pressure equal to 1.24 kPa was monitored at point P3, followed by 0.56 kPa at point P2 and 0.26 kPa at point P1. The rapid increase of pore water pressure was consistent with the heaviest rainfall intensity among the entire rainfall period. Given that there was no obvious change of pore water pressure before the global slide failure, the method of predicting slope failure by monitoring changes in pore water pressure was not suitable for the earthen slope under unimodal rainfall pattern.

Thereby, the increment of PWP value depending on the location and rainfall intensity. The method of predicting slope failure by monitoring changes in pore water pressure was suitable for constant rainfall pattern, but not suggested for unimodal rainfall pattern.

5.5 Rainfall infiltration rate and seepage length

Fig.9 shows the infiltrated rainwater into the slope over time for different rainfall patterns. The length of the seepage path referred to the length of the red seepage line, as shown in Fig. 4 and Fig. 5. By recording the video of the entire experiment in real-time, the development of the red seepage line can be measured in every minute. Then, the rainfall infiltration rate can be calculated based on the velocity development of the red seepage line throughout the experiment.

During the experimental model under the constant rainfall pattern, all the rainwater infiltrated into the slope and there was no runoff on the slope surface (Fig.4), since rainfall intensity was always smaller than the saturated coefficient of permeability (k_s). The maximum rainfall infiltration rate was measured in the unsaturated slope at the early stage. Then, the infiltration rate slowly decreased during rainfall and kept at a constant value in the end. Meanwhile, the seepage length increased linearly to 827 mm in the experiment tank.

For the slope under the unimodal rainfall pattern, the variation of infiltration rate was consistent with the rainfall intensity. The infiltration rate increased up to its maximum value during the heaviest rainfall intensity, accompanying the occurrence of larger seepage force in the inner of slope soil. Larger erosive force on the slope and seepage force inside the soil directly led to the global slope failure in a short time. Besides, the seepage length increased to 1000 mm with a characteristic of nonlinearity.

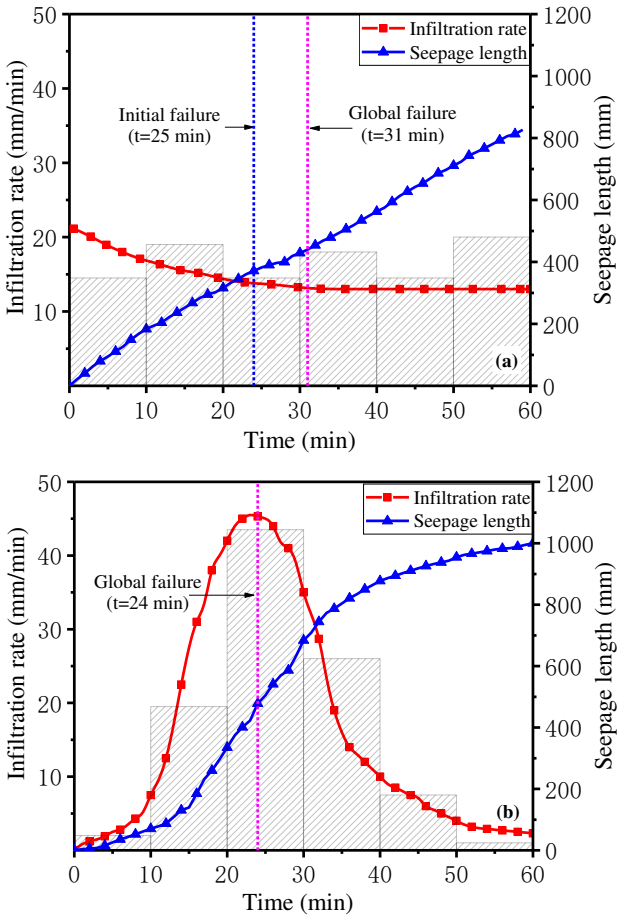

Figure 9. Rainfall infiltration rate and seepage length under different rainfall patterns.

6 CONCLUSIONS

To investigate the effect of different rainfall patterns on earthen slope, a series of laboratory experiments with the same cumulative rainfall (200 mm) were carried out on small-scale slope models. Slope failure process, failure evolution modes, settlement of slope crest, pore water pressures, and rainfall infiltration rate were measured during the rainfall experiments. The major findings and conclusions obtained are as follows:

(1) Two types of failures: retrogressive failure and translational failure, were observed. The failure evolution modes were affected by the rainfall patterns. In the case of the constant rainfall pattern, a saturated area formed firstly near the slope toe, followed by the occurrence

of initial flow slide failure as the effect of reduction in effective stress. As the sequential failures occurred, the displacement influence area gradually expanded to the slope crest until the global slide failure happened. While, in the case of the unimodal rainfall pattern, higher rainfall intensity during the peak rainfall stage reduced the shear strength of the slope soil, which was insufficient to retain the stability of the entire slope, resulting in a translational failure suddenly.

(2) Under the same cumulative rainfall (200 mm), it was obvious that the unimodal rainfall pattern was more harmful to earthen slope than the constant rainfall pattern, based on the erosion area of slope.

(3) Taking the method of monitoring the settlement displacement of slope crest to predict the slope failure was available for the slope under the constant rainfall pattern. But it was not recommended in case of the unimodal rainfall pattern since its global slide failure with a characteristic of suddenness.

(4) It was found that the increase of pore water pressure correlated well with the occurrence of slope failure. In the case of the constant rainfall pattern, the pore water pressure would rise slightly before the initial failure. While, in the case of unimodal rainfall pattern the pore water pressure was nearly constant in the early period. Thereby, the method of predicting slope failure by monitoring changes in pore water pressure was more applicable for the slope under the constant rainfall pattern than the unimodal rainfall pattern.

(5) During rainfall with a constant intensity, the maximum rainfall infiltration rate at the beginning decreased slowly and kept a constant value in the end. While, in the case of a unimodal pattern, the change of infiltration rate correlated well with the rainfall intensity during the experiment.

ACKNOWLEDGMENT

The financial support from the National Key R&D Program of China (2016YFC0800200) is gratefully acknowledged.

REFERENCES

Askrinejad, A., Casini, F., Bischof, P., Beck, A., & Springman, S., (2012). *"Rainfall induced instabilities: a field experiment on a silty sand slope in northern switzerland"*. Rivistaltaliana Di Geotecnica, 3.

Brunetti, M. T., Peruccacci, S., Rossi, M., Luciani, S., Valigi, D., & Guzzetti, F., (2010). *"Rainfall thresholds for the possible occurrence of landslides in Italy"*. Natural Hazards and Earth System Science, 10(3), 447-458.

Caine, N. (1980). "*The Rainfall Intensity: Duration Control of Shallow Landslides and Debris Flows*". Geografiska Annaler. Series A, Physical Geography 62(1-2):23-27.

Casadei, M., Dietrich, W. E., & Miller, N. L.. (2003) *"Testing a model for predicting the timing and location of shallow landslide initiation in soil - mantled landscapes"*. Earth Surface Processes and Landforms, 28.

Casini, F., Jommi, C., & Springman, S., (2010). *"A laboratory investigation on an undisturbed silty sand from a slope prone to landsliding"*. Granular Matter, 12(3), 303-316.

Chen, H. K., Wei L., Tan L., (2012). *"Review of research on empirical rainfall threshold of rainfall-induced landslide"*. Journal of Chongqing Jiaotong University Natural Science, 31(5):990-996.

Guzzetti, F., Peruccacci, S., Rossi, M., & Stark, C. P., (2007). *"Rainfall thresholds for the initiation of landslides in central and southern Europe"*. Meteorology and Atmospheric Physics, 98(3-4), 239-267.

Iverson, R. M., (2000). *"Landslide triggering by rain infiltration"*. Water Resources Research 36(7).

Keefer, D. K., Wilson, R. C., Mark, R. K., Brabb, E. E. , Brown, W. M., & Ellen, S. D., et al. (1987). *"Real-time landslide warning during heavy rainfall"*. Science, 238(4829), 921-925.

Li, Y., Meng, H., Dong Y., (2004).*"Main types and characterisitics of geo-hazard in China—Based on the results of geo-hazard survey in 290 counties"*. The Chinese Journal of Geological Hazard and Control,15(2): 32 – 37.

Ochiai, H., Okada, Y., Furuya, G., Okura, Y., Matsui, T., & Sammori, T., et al. (2004). *"A fluidized landslide on a natural slope by artificial rainfall"*. Landslides, 1(3), 211-219.

Stark, T. D. and Hussain, M. (2013). "*Drained Shear Strength Correlations for Slope Stability Analyses*", J. of Geotechnical Engineering, ASCE, 139(6).853-862.

Stark, T. D., Baghdady, A. K., Hungr, O., & Aaron, J., (2017). *"Case study: OSO, landslide of march 22, 2014—material properties and failure mechanism."* Journal of Geotechnical and Geoenvironmental Engineering, 143(5), 05017001.

Tan, Y., Jiang, W., Luo, W., Lu, Y., & Xu, C., (2018). "*Longitudinal sliding event during excavation of feng-qi station of hangzhou metro line 1: post-failure investigation*". Journal of Performance of Constructed Facilities, 32(4), 04018039.

Zhong, Y. Q., (1998). *"Landslide related to rainfall and its forecasting".* The Chinese Journal of Geological Hazard and Control, 9(4):81-86.